Journal of the Korean Crystal Growth and Crystal Technology
Vol. 14, No. 6 (2004) 236-243

Characterization of via etch by enhanced reactive ion etching

Y.G. Bae and C.S. Park†

Department of Electronic Engineering, Hanseo University, Chung-Nam 356-820, Korea

(Received June 9, 2004)
(Accepted October 12, 2004)

Abstract The oxide etching process was characterized in a magnetically enhanced reactive ion etching (MERIE) reactor with a CHF_3/CF_4 gas chemistry. A statistical experimental design plus one center point was used to characterize relationships between process factors and etch response. The etch response modeled are etch rate, etch selectivity to TiN and uniformity. Etching uniformity was improved with increasing CF_4 flow ratio, increasing source power, and increasing pressure depending on source power. Characterization of via etching in CHF_3/CF_4 MERIE using neural networks was successfully executed giving to highly valuable information about etching mechanism and optimum etching condition. It was found that etching uniformity was closely related to surface polymerization, DC bias, TiN and uniformity.

Key words Oxide etching, Uniformity, Via etching, Etching mechanism

1. Introduction

Plasma etching has gained widespread use in the manufacture of very large scale integrated circuits [1]. It is due to its advantages of anisotropic pattern formation, high-fidelity pattern transfer and processing at relatively low temperature. As device dimensions in ultra-large-scale integration (ULSI) continue to shrink, plasma etching will be an essential process in many critical fabrication steps, such as gate poly, contact & via, and metal etch process [2]. At the same time, requirements for etching selectivity, line-width control, etching uniformity, and etched profile have become more stringent and more difficult to meet [3]. In particular, sub-micron pattern and high aspect ratios (> 10 : 1) have created unexpected problems in via etching for inter-metal connections. Accordingly, in order to obtain low via resistance and wide process window, uniformity and selectivity to TiN of etched IMD films should be strictly controlled.

Optimizing via-etch process is extremely difficult due to complex relationships between process factors and etch responses as well as some trade-offs between the responses. It is therefore highly demanded to develop computer simulation models to form via holes in a cost-effective way. Historically, plasma models have been developed using the first principle physics involving continuity, momentum balance, and energy balance inside a high frequency, high intensity electric or magnetic or both fields. Due to the lack of understanding of physical and chemical processes, however, they are subject to many simplifying assumptions, which often result in somewhat larger discrepancy between model predictions and actual measurements. As an alternative, an adaptive learning technique which utilizes neural networks combined with statistical experimental design has been used to understand underlying etch mechanisms [4-7]. Neural net plasma models once demonstrated improved prediction over statistical response surface models in modeling plasma etch processes [6-8]. An oxide etch process was characterized in a magnetically enhanced reactive ion etching (MERIE) reactor with CHF_3/CF_4 gas chemistry. A statistical experimental design plus one center point was used to characterize relationships between process factors and etch responses. The factors that were varied in the design include rf power, pressure, and gas composition. The etch responses modeled are etch rate, etch selectivity to TiN, and uniformity. The developed models were then utilized to produce 3D response plots.

Etching of SiO_2 mainly depends on F density and ion bombardment. SiO_2 etch selectivity to TiN sensitively depends on F density in plasma and ion bombardment effects resulting in high etch selectivity with the increase of pressure at relatively high DC bias voltage and high CF_4 flow ratio. Etching uniformity was improved with increasing CF_4 flow ratio in gas mixture, increasing source power, and higher pressure depending on gas composition.

Characterization of via etching in CHF_3/CF_4 MERIE using neural networks was successfully executed giving

†Corresponding author
Tel: +82-41-660-1413
Fax: +82-41-660-1119
E-mail: pcs98@hanseo.ac.kr

to highly valuable information about etching mechanism and optimum etching condition with very economical and effective way.

In this study, neural network is used to model characteristics of oxide film etched in $CHF_3/CF_4/Ar$ gas chemistry. A magnetically enhanced reactive ion etcher (MERIE) was used for etching. A statistical experimental design was employed to systematically characterize relationships between process factors and etch responses. The factors that were varied in the design include rf power, pressure, and CHF_3 and CF_4 flow rates. Apart from conventional etch rate, etch uniformity and selectivity to TiN are particularly modeled.

2. Experiment

2.1. Apparatus

A schematic diagram of the MERIE system (P-5000MxP) used for oxide etching is shown in Fig. 1. With the upper plate grounded, the lower one is capacitively coupled to a 13.56 MHz RF power supply via matching network. Magnetic field parallel to the lower electrode is generated by the electromagnetic coils mounted around outside the reactor chamber. During the etching, the substrate holder temperature was held at 20°C.

2.2. Experimental Design

In order to characterize relationships between process factors and etch characteristics, a statistical full factorial design [10] was employed with one center point. The factors that were varied include rf power, pressure,

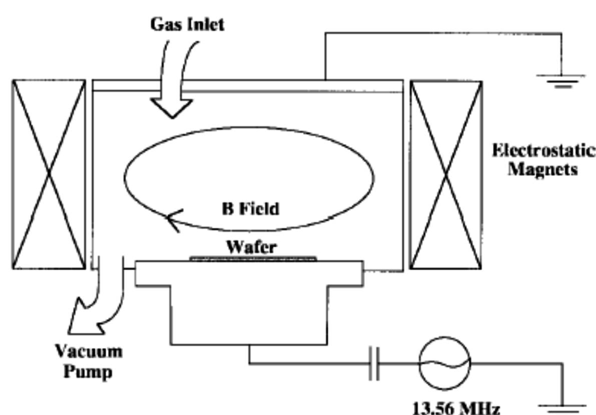

Fig. 1. Schematic diagram of magnetically enhanced RIE system (P-5000MxP).

Table 1
Range and values of main independent variables and constants for MERIE etching process

Parameter	Range	Units
CHF_3	20~80	sccm
CF_4	10~40	sccm
Pressure	50~200	mTorr
RF power	300~800	Watts

CHF_3 and CF_4 flow rates. Experimental ranges of factors are contained in Table 1. Resultant 9 experiments were used to train neural networks and trained networks were tested on 8 experiments were additionally conducted and thus a total of 17 experiments were performed to develop a predictive etch model.

2.3. Experiments

Test patterns were fabricated on (100) oriented Si substrates, which were doped with Boron (1~30 Ω-cm) and chemically cleaned for 600 sec using 4 H_2SO_4 : 1 H_2O_2 mixture solution at the temperature of 110°C. This was then followed by de-ionized water rinse prior to plasma enhanced chemical vapor deposition (PECVD) growth. Oxide films of about 900-nm-thick were prepared on chemically pre-cleaned (100) silicon by the reaction of SiH_4 and N_2O in a plasma-enhanced CVD reactor at the substrate temperature of 400°C and reaction pressure of 3 Torr. Using a spin coater, 1.02-μm thick photoresist-film was coated at the RPM of 4000 and subsequently soft-baked for 90 sec at the temperature of 90°C on the hot-plate in the track system (TEL Mark-Vz). PR pattern with equal lines & spaces and holes was formed using i-line Nikon stepper (NSR2205i11D). Developed samples were subsequently hard-baked at 120°C for 30 min in the convection oven.

The etching experiments were carried out in a MERIE reactor equipped with an optical emission spectrometer to analyze active species in the gas phase. Range and values of main independent variables and constants for MERIE etching process are shown in Table 1. Film thickness was measured using a NanoSpec 3000 spectroscopic reflectometer. Etch rate data were extracted at no patterned region by dividing etched film thickness by etch time.

The analysis in the gas mixtures was carried out using in-situ optical emission spectroscopy (OES) which was built-in in the system. The emission light from the glow discharge of different feed gas mixtures was focused with a quartz lens and introduced into a monochroma-

tor. The OES apparatus for experiments consisted of a photomultiplier tube and a conventional photocounting system comprising a discriminator, a multi-channel scaler, and a personal computer. Optical emission measurements were made in the range of wavelength between 200 and 800 nm with a resolution of 0.25 nm. During optical emission measurements, a certain amount of Ar gas (90 sccm) was introduced into the reaction chamber to provide reference peak.

3. Neural Networks

Among the various paradigms of artificial neural networks, the back-propagation neural network (BPNN) was employed for this plasma modeling due to its proven high accuracy in learning nonlinear process data. A typical architecture of BPNN is exhibited in Fig. 2.

BPNN consists of one or more layers of neurons: input layer, hidden layer, and output layer. The input layer receives external information such as that represented by the three adjustable equipment parameters in Table 1. The output layer transmits the data and thus corresponds to the various plasma attributes (electron density, electron temperature, and plasma potential). In this study, the number of neurons in the output layer was set to unity since each attribute was modeled one by one. BPNN also incorporates "hidden" layers of neurons that do not interact with the outside world, but assists in performing nonlinear feature extraction on the data provided by the input and output layers. Activation level (or firing strength) of a neuron is determined by a nonlinear sigmoid function denoted as:

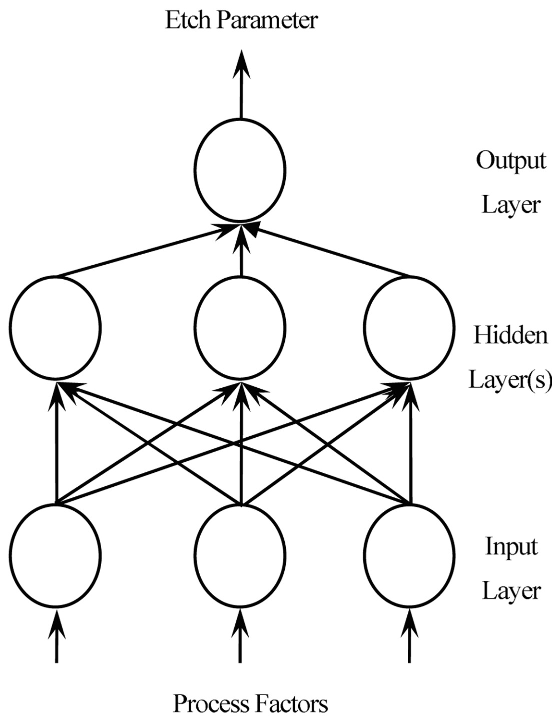

Fig. 2. A schematic diagram of backpropagation neural network.

$$out_{i,k} = \frac{1}{1 + e^{-int_{i,k}}} \tag{1}$$

where $int_{i,k}$ and $out_{i,k}$ indicate the weighted input to the *i*th neuron in the *k*th layer and output from that neuron, respectively.

The BP algorithm by which the network is trained begins with a random set of weights (i.e. connection strengths between neurons). An input vector, which has been normalized to lie in the interval between −1 and 1, is then presented to the network, and the output is calculated using initial weight matrix. Next, the calculated (or predicted) output is compared to the actually measured output, and the squared difference between the two determines the system error. The Euclidean distance in the weight space the network attempts to minimize is the accumulated error (E) of all the input-output pairs, which is expressed as:

$$E = 0.5 \sum_{j=1}^{q} (d_j - out_j)^2 \tag{2}$$

where q is the number of output neurons, d_j is the desired output of the *j*th neuron in the output layer, and out_j is the calculated output of that same neuron. In BP algorithm, this error is to be minimized via the *gradient descent* optimization, in which the weights are adjusted in the direction of decreasing the E in (2). A basic weight update scheme, commonly known as the generalized delta rule is expressed as:

$$W_{i,j,k}(m+1) = W_{i,j,k}(m) + \eta \Delta W_{i,j,k}(m) \tag{3}$$

where $W_{i,j,k}$ is the connection strength between the *j*th neuron in the layer (k − 1) and the *i*th neuron in the layer k, and $\Delta W_{i,j,k}$ is the calculated change in the weight to minimize the E in (2) and defined as:

$$\Delta W_{i,j,k} = -\frac{\partial E}{\partial W_{i,j,k}} \tag{4}$$

Other m and η indicate the iteration number and an adjustable parameter so called "learning rate", respectively. By adjusting weighted connections recursively using the rule in (4) for all the units in the network, the accumulated over all the input vectors is to be minimized.

4. Results and Discussion

4.1. Model Development

Using neural networks, predictive etch models were developed. Among many paradigms, backpropagation neural network (BPNN) was used due to its popularity in plasma-driven processes [4-8]. BPNN was trained on the nine experiments obtained from 2^{4-1} experiment and one center point. Trained model was then tested on additionally conducted eight experiments. Although many training variables are typically involved, in this study, only one hidden neuron variable was optimized under random initial weights. The number of hidden neurons was varied from 3 to 6 experimentally, As detailed in previous study [9], multiple models of 200 were generated for a fixed hidden neurons to take into account randomness in initial weight distribution. Only one model with minimum prediction error was then selected out of 200 local minima and this model was used to make various 3-D plots. The hidden neurons optimized are 6, 5, and 5 for etch rate, etch uniformity, and selectivity to TiN, respectively. Prediction errors corresponding to optimal hidden neurons are 149.8 Å/min, 0.807, and 26.30 for etch rate, etch uniformity, and selectivity to TiN, respectively. Here, the prediction error was quantified with the root-mean squared error metric.

4.2. Etch Rate

Figure 3 plots etch rates of oxide with various CF_4 and CHF_3 gas flow rates at the pressure of 125 mTorr and RF power of 550 W. This figure shows that etch rates of oxide films increase with increasing CF_4 flow rate and decreasing CHF_3 one. In general, it is known that F radicals to be generated in the plasma react with oxide and form compounds of COF_2 and SiF_4, finally having a dominant influence on etching oxide films. At the same time, the increase of CHF_3 flow rate forms a compound of HF in the plasma, finally decreasing the density of F radicals in the plasma. Therefore, the increase of CF_4 flow rate and the decrease of CHF_3 one enhances the density of F radicals in the plasma, increasing etch rates of oxide films.

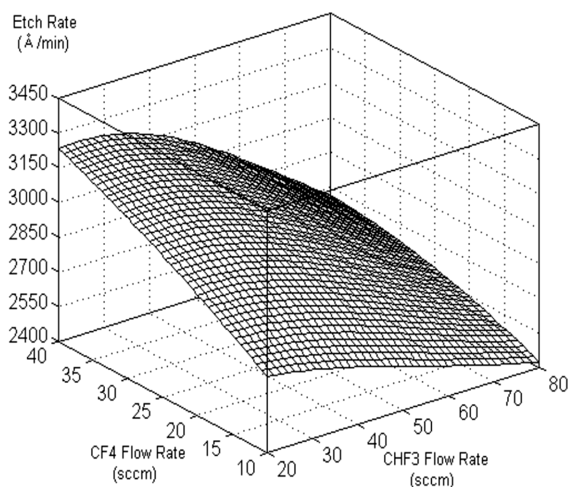

Fig. 3. Etch rates with various CF_4 and CHF_3 gas flow rates.

To get the knowledge about reaction mechanism related to CF_4/CHF_3 gas composition, active species to be generated in the plasma and etch residues on etched SiO_2 surface as a function of gas composition were analyzed by using optical emission spectroscopy (OES) and x-ray photoelectron spectroscopy (XPS), respectively. XPS (ESCALAB 200R_VG Scientific) analyses have been performed by collecting C1s and F1s regions at pass energies of 20 eV with AlKα x-ray source at take-off angles of 90°. Relative peak intensities for C1s (290~295 eV) and F1s (694 eV) in XPS analysis were normalized with respect to the highest relative intensity.

Figure 4(a) shows the variation of F, H, and CF_2 in the plasma as a function of $CF_4/(CF_4 + CHF_3)$ flow ratio at the condition of source power 550 Watts and pressure 125 mTorr. In the regimes of I-II, while emission intensity of F in OES analysis was continuously decreased with the increase of CF_4 flow ratio, maximal emission intensity of H and CF_2 species was obtained at a CF_4 flow ratio of 0.13. It is assumed that the increase of H and CF_2 in the regime I was induced by fast polymer decomposition with the increase of CF_4 flow ratio.

In the regime III, emission intensity of F and CF_2 slowly increase, but emission intensity of H does not increase because of the decrease of CHF_3 flow ratio. It is assumed that F radical is intensively participating in the reaction of polymer decomposition and SiO_2 etching with the increase of CF_4 flow ratio in the regime I. It is confirmed by sharp decrease of C1s and F1s intensity in Fig. 4(b) and steep increase of SiO_2 etch rate in Fig. 4(c). The 4 nm thick CF_x residue formed on surface etched by using CHF_3/C_2F_6 gas in reactive ion etching was easily removed by NF_3 plasma treatment. Therefore, with the increase of CF_4 flow ratio, decrease of C1s intensity in Fig. 4(b) well agrees with H. Park's results. In regime II of Fig. 4(a), fast decrease of H intensity was caused by the reaction with F for HF formation and dilution of CHF_3 in gas mixture. CF_2 was generated by not only dissociation of CF_4 and CHF_3, respectively, but also reaction of CF_3 with H. Therefore,

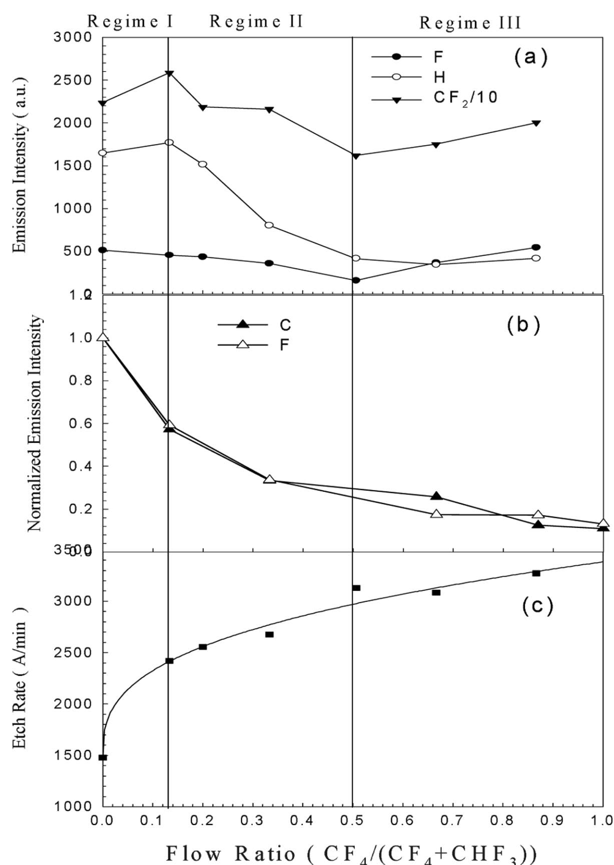

Fig. 4. Optical emission intensity of F, H, CF_2 in plasma phase (a), normalized emission intensity of C 1s and F1s on etched SiO_2 surface by XPS (b), and blank etch rate of SiO_2 as a function of CF_4 flow ratio in CF4/(CF_4 + CHF_3) gas mixture.

intensity of CF_2 was proportional to H intensity in the regime I-II. Increase of F in regime III was caused by increase of CF_4 flow ratio and decrease of polymer deposition, while increase of CF_2 in regime III was caused by increase of CF_4 flow ratio and competitive reaction with increased F on SiO_2 surface. We speculate about the role of F, H, and CF_x radical to explain the etch phenomenon in each regime. Roles of F radical are etching of polymer layer and SiO_2, H radical is scavenging F radical by forming HF compound [9], which is ineffective species for SiO_2 etching, inhibiting surface adsorption of F radical by competitive surface adsorption while enhancing the surface polymerization with co-adsorbed CF_x and CHF_x species.

From these results, in regime I, we could infer that etching of SiO_2 mainly occurred at the interface between thick-polymer and SiO_2 by the diffusion of active species and ion bombardment. Therefore, etch rate of SiO_2 steeply increase with the decrease of polymer thickness caused by increasing CF_4 flow ratio. In regime III, because of thin polymer layer, etch rate of SiO_2 mainly occurred on SiO_2 surface depending on F density. In regime II, etching of SiO_2 proceeds with a little polymer deposition depending on density of active species and ion bombardment.

Therefore, according to gas composition of CF_4/(CF_4 + CHF_3), etching mode of oxide film converted from thin polymer layer and F species dominated chemical reaction at high CF_4 ratio in gas mixture to thick polymer layer and F species density dependent reaction at low CF_4 ratio in gas mixture through the transient region.

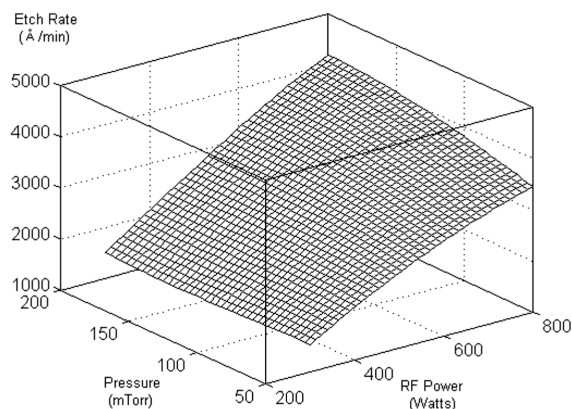

Fig. 5. Etch rates with various pressure and RF power.

Figure 5 plots etch rates of oxide with various pressure and RF power at the CF_4 flow rate of 50 sccm and CHF_3 of 25 sccm. Generally, etch rates depend on chemical reactions by radicals and physical effects by ion bombardments. Meanwhile, ion bombardment effects rely on ion densities and DC bias voltages.

It is well known that the increase of pressure increases the densities of F radicals at sufficient RF power, but on the contrary, decreases DC bias voltage. Actually, the DC bias greatly decreased from −669 V to −528 V as the pressure was increased from 50 mTorr to 200 mTorr at the 550 W RF power, and 50 and 25 sccm for CHF_3/CF_4. As the results, etch rate of SiO_2 slightly decreased with the increase of pressure at RF power of 300 Watts. On the contrary, at RF power of 800 W, although DC bias voltage with the increase of pressure decreased, ion bombardment energy for etching reaction was still higher enough. Therefore, etch rate of SiO_2 increase with the increase of pressure.

Meanwhile, the increase of RF power increases the densities of F radicals and DC bias voltage, together. Therefore chemical reactions by radicals and physical effects by ion bombardments are increased simultaneously. As a result, etch rates increase sharply with increasing RF power. From this result, we can find out that RF power has larger influence on etch rates of

oxide films than pressure. In this figure, we can also find out that etch rates at the pressure of 200 mTorr more sharply increase than those at 50 mTorr. This difference seems to be due to the supply of active species at each pressure. That is, while etch rates sharply increase with RF power at the pressure of 200 mTorr due to the sufficient supply of active etching species, etch rates increases slower at the chamber pressure of 50 mTorr due to the deficient supply of active etching species.

4.3. Etch Selectivity

Figure 6 plots etching selectivity of SiO_2 films over TiN films with various RF power and CF_4 gas flow rates with constant Ar and CHF_3 gas flow rates of 90 and 50 sccm, respectively. Prior to this work, we examined the etching rate of TiN films with various CF_4 gas flow rates and found out the increase of TiN etch rate with increasing CF_4 gas flow rates. The report described that TiF_x (x = 3~4) was etching by-products and the formation of TiF_x (x = 3~4) depended on F radical density. This explanation indicates that the etching rate of TiN increases with increasing CF_4 gas flow rate. At the same time, it was also found that the etch rate of oxide films increased with increasing CF_4 gas flow rate.

This figure shows the increase of the selectivity with increasing CF_4 gas flow rates at 800 W RF power. This means that the etching rate of oxide films sharply increases as compared to that of TiN films within the experimental range of this study. This difference seemed to be due to the volatility of etching by-products, such as SiF_4 and TiF_x. While SiF_4, etching by-product of oxide films, has a high volatility (vapor pressure is 1 mmHg @ -144°C), boiling points of TiF_3 and TiF_4, etching by-products of TiN films, are 1400°C and 248°C, respectively. This data means that the vaporization of TiF_x is harder than that of SiF_4.

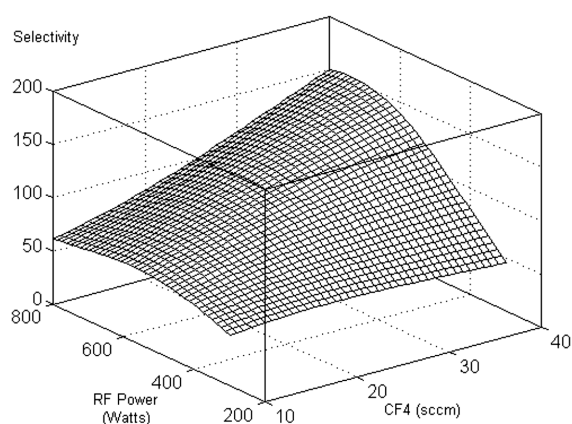

Fig. 6. Etching selectivity of SiO_2/TiN films with various RF power and CF_4 gas flow rates.

At RF power of 300 W, etch selectivity of SiO_2/TiN was scarcely varied with the increase of CF_4 ratio in the gas mixture. This reveals that at relatively smaller RF power etch rate of SiO_2 and TiN film is not largely affected by increasing F intensity.

At RF power of 800 W, etch selectivity of SiO_2/TiN increased with the increase of CF_4 flow rate ratio in the gas mixture. At high RF power condition, etch rate of SiO_2 sharply increase with the increase of CF_4 gas flow ratio because SiO_2 film has a self containing O-atom, which makes less sensitive for surface polymerization compared to TiN film, and high volatility of etching by-products. With higher CF_4 flow-rate ratio at high source power, the difference of etching reaction was only volatility of etching by-products. Therefore, at the CF_4 gas flow ratio higher than 0.5, etch selectivity of SiO_2/TiN was decreased, although it was not seen in Fig. 6. At CF_4 flow rate of 10 sccm, etch selectivity of SiO_2/TiN slowly increases at RF power less than 500 Watts and then remains constant at the RF power more than 500 W. In this low power regime, slow increase of SiO_2 etch selectivity to TiN was caused by self-containing O atom and high volatility of SiF4 compared to TiF_x (x = 3~4). At high power regime, both SiO_2 and TiN was etched by ion bombardment and suffered from low etch rate due to intense surface polymerization and low density of F species. Therefore, etch selectivity of SiO_2/TiN does not increase at the range of high RF power and high CHF_3 flow rate.

At CF_4 flow rate of 40 sccm, etch selectivity of SiO_2/TiN increased for RF power less than 630 Watts and remained constant at the RF power more than 630 Watts. At the low CHF_3 gas ratio and 300~630 W RF power regimes, carbon-containing polymer deposition was not actively occurred on both film surfaces. Therefore, increase of etch rate of SiO_2 film, which has self-containing O-atom and high volatility of etching by-product, is faster than that of TiN film. However, increasing rate of TiN etch rate is steep at the RF power more than 630 W because ion bombardment energy is sufficient for the removal of etch by-products. Therefore increasing rate of etch selectivity was slow down and finally decreased. Maximal etch-selectivity could be obtained at the condition of 600~700 W RF power and high CF_4 flow ratio of 0.5 in gas mixture. Therefore, SiO_2 etch selectivity to TiN sensitively depends on F density in plasma and ion bombardment effects.

From these results, etching of TiN was suffered from

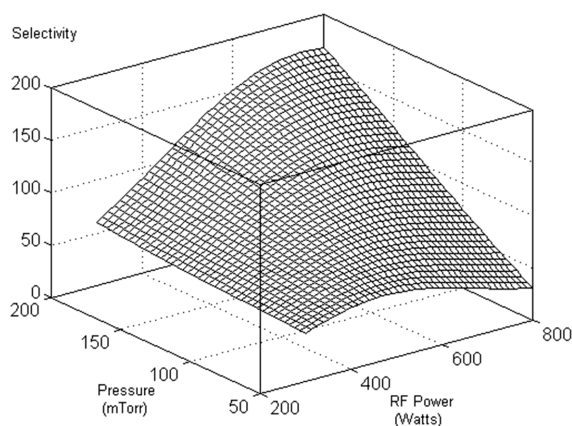

Fig. 7. Etching selectivity of TiN films with various pressure and RF power.

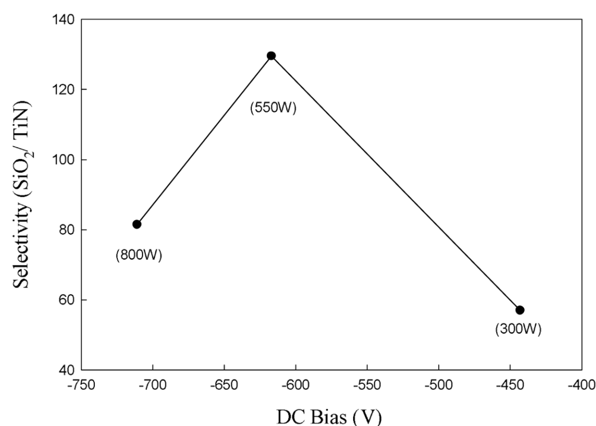

Fig. 8. Etch selectivity of (SiO_2/TiN) as a function of DC Bias voltage (Pressure = 125 mTorr, M_Field = 50 Gauss, CHF_3/CF_4/Ar = 50/25/90 sccm).

surface polymerization and low volatility of etch by-product such as TiF_3 and TiF_4. On the other hand, etch of SiO_2 depends on ion bombardment and F dominated etching rather than surface polymerization because oxygen content of SiO_2 film partly participate in polymer removal reaction.

Figure 7 plots etching selectivity of TiN films with various pressure and RF power. It is exhibited in Fig. 7 that the selectivity increases with increasing chamber pressure and increasing RF power. To understand this, it was examined the etching selectivity of SiO_2/TiN as a function of DC bias voltage with a fixed pressure. In this case, DC bias voltage was controlled by RF power. In Fig. 8, where a maximal etch selectivity of 130 was obtained at DC bias voltage of −617 V. Above −617 V, etch selectivity of SiO_2/TiN decreased sharply. Etch rate of SiO_2 sharply increase with the increase of DC bias voltage, and then increasing rate of SiO_2 etch rate slows down with the insufficient supply of etching species. However, etch rate of TiN was not influenced that much by the increase of DC bias voltage until −617 V because of low volatility of etch by-products. Above the −617 V, etch rate of TiN sharply increased, therefore etch selectivity of SiO_2/TiN also sharply decreased.

The increase of pressure, electron temperature which was a major factor for dissociation of reaction gas, sharply decreased and resulted in CF_x abundance in CF_4 plasma. Therefore, density behavior of F was explained by electron temperature, which depends on RF power and pressure. Therefore, with the increase of pressure, polymerization reaction of both gas phase and surface was actively occurred in spite of maintaining high dc bias voltage, inhibiting surface reaction between TiN and F radical as well as removal of TiN etching by-products.

But SiO_2 etch more depend on dc bias and F density with high volatility of SiF_4 rather than CF_x abundance, result in high etch selectivity with the increase of pressure at relatively high DC bias voltage.

In this work, we found a reduction in TiN etch rate with increasing pressure. With the increase of chamber pressure, we also found a decrease in the DC bias voltage with increasing pressure. Actually, the DC bias greatly decreased from −669 V to −528 V as the pressure was increased from 50 mTorr to 200 mTorr at the 550 W RF power, and 50 and 25 sccm for CHF_3/CF_4. And etch rate of TiN sharply increase at the higher values of −600 V DC bias voltage. As opposed to this, etch rate of SiO_2 sharply increased with increasing chamber pressure within the DC bias voltage range of −500 V~ −700 V.

4.4. Etch Uniformity

Figure 9 plots etch uniformity with CF_4 and CHF_3 flow rates. This figure indicates that the etch uniformity is enhanced with increasing CF_4 flow rate and decreasing CHF_3 flow rate. It is generally known that the uniformity becomes worse with increasing thickness of a polymer layer which is largely influenced by $CF_x(x < 3)$ species. At the same time, $CF_x(x < 3)$ species is reduced with increasing CF_4 flow rate and decreasing CHF_3 one. As a result, the etch uniformity is improved with increasing CF_4 flow rate and decreasing CHF_3 one.

Figure 10 plots the etching uniformity with various pressure and RF power. This figure shows that uniformity is improved with increasing RF power and pressure.

The improvement of the uniformity with increasing

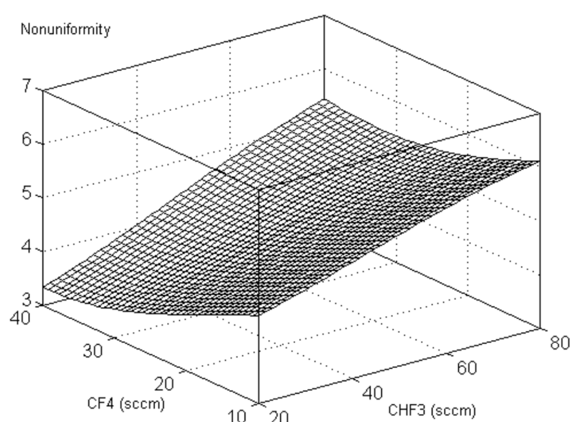

Fig. 9. Etch uniformity with CF_4 and CHF_3 flow rates.

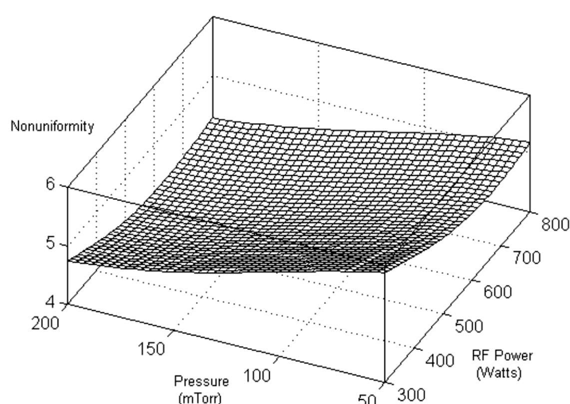

Fig. 10. Etching uniformity with various pressure and RF power.

pressure can be inferred from uniform distributions of etching species in the etching chamber. At the same time, the uniformity improved with increasing RF power agrees with the formation of polymer layer on the etching surface had been closely related to the effect of ion bombardment. That is, the increase of RF power brings about an increase in DC bias voltage and then reduces the polymer thickness on the etching surface, finally improving the uniformity. Therefore etching uniformity was closely related to surface polymerization, DC bias, and density of active species in plasma.

5. Conclusions

A oxide etch process was characterized in a magnetically enhanced reactive ion etching (MERIE) reactor with a CHF_3/CF_4 gas chemistry. A statistical experimental design plus one center point was used to characterize relationships between process factors and etch responses. The factors that were varied in the design include rf power, pressure, and gas composition. The etch responses modeled are etch rate, etch selectivity to TiN and uniformity. Etching of SiO_2 and TiN mainly depends on F density and ion bombardment. Etching of TiN more sensitively depends on F density because active species for polymer decomposition on surface and TiN etching are only F radical and dc bias voltage because etch by-products such as TiF_3 or TiF_4 have higher boiling point. Therefore, process condition for high selectivity was proposed for 0.3~0.5 CF_4 flow ratio and -600 V~-650 V DC bias voltage depending on pressure. Etching uniformity was improved with increasing CF_4 flow ratio, increasing source power, and increasing pressure depending on source power. Characterization of via etching in CHF_3/CF_4 MERIE using neural networks was successfully executed giving to highly valuable information about etching mechanism and optimum etching condition with very economical and effective way.

References

[1] R.J. Schutz, in VLSI Technology, 2nd ed., edited by S.M. Sze (McGraw-Hill, New York, 1988).
[2] J.M. Cook and K.G. Donohoe, “Etching issues at 0.35 μm and below”, Solid State Technolog 34 (1991) 119.
[3] B. Kim, J. Sun, C. Choi, D. Lee and Y. Seol, “Use of neural networks to model low-temperature tungsten etch characteristics in high density SF_6 plasma”, J. Vac. Sci. Technol. A18 (2000) 417.
[4] C.D. Himmel and G.S. May, “Advantages of plasma etch modeling using neural networks over statistical techniques”, IEEE Trans. Semicond. Manufact. 6 (1993) 103.
[5] B. Kim and G.T. Park, “Modeling plasma equipment using neural networks”, IEEE Trans Plasma Sci. 29 (2001) 8.
[6] S.H. Oh and S.Y. Lee, “An adaptive learning rate with limited error signals for training of multilayer perceptrons”, ETRI Journal 22(4) (2000) 40.
[7] D.C. Mongomery, Design and Analysis of Experiments (John Wiley & Sons, 1991).
[8] D.E. Rummelhart and J.L. McClelland, Parallel Distributed Processing (Cambridge, M.I.T. Press, 1986).
[9] B. Kim and G.S. May, “An optimal neural network process model for plasma etching”, IEEE Trans. Semicond. Manufact. 7 (1994) 12.